

Modelling and evaluating a solar pyrolysis system

Sánchez, M, Nixon, J & Clifford, B

Author post-print (accepted) deposited by Coventry University's Repository

Original citation & hyperlink:

Sánchez, M, Nixon, J & Clifford, B 2018, 'Modelling and evaluating a solar pyrolysis system' *Renewable Energy*, vol 116, pp. 630-638

<https://dx.doi.org/10.1016/j.renene.2017.10.023>

DOI 10.1016/j.renene.2017.10.023

ISSN 0960-1481

ESSN 1879-0682

Publisher: Elsevier

NOTICE: this is the author's version of a work that was accepted for publication in *Renewable Energy*. Changes resulting from the publishing process, such as peer review, editing, corrections, structural formatting, and other quality control mechanisms may not be reflected in this document. Changes may have been made to this work since it was submitted for publication. A definitive version was subsequently published in *Renewable Energy*, [116, (2017)] DOI: 10.1016/j.renene.2017.10.023

© 2017, Elsevier. Licensed under the Creative Commons Attribution-NonCommercial-NoDerivatives 4.0 International

<http://creativecommons.org/licenses/by-nc-nd/4.0/>

Copyright © and Moral Rights are retained by the author(s) and/ or other copyright owners. A copy can be downloaded for personal non-commercial research or study, without prior permission or charge. This item cannot be reproduced or quoted extensively from without first obtaining permission in writing from the copyright holder(s). The content must not be changed in any way or sold commercially in any format or medium without the formal permission of the copyright holders.

This document is the author's post-print version, incorporating any revisions agreed during the peer-review process. Some differences between the published version and this version may remain and you are advised to consult the published version if you wish to cite from it.

1 Modelling and evaluating a solar pyrolysis system

2
3 M. Sánchez^a, B. Clifford^a and J. D. Nixon^{b*}

4
5 ^aKingston University, Faculty of Science, Engineering and Computing, Roehampton Vale
6 campus, London, SW15 3DW, UK

7 ^bCoventry University, Faculty of Engineering, Environment and Computing, Coventry, CV1
8 2JH, UK

9 *corresponding author, E-mail: jonathan.nixon@coventry.ac.uk; Tel.: 024 7688 7688

11 Abstract

12 This study investigates the use of solar energy for producing biofuels through pyrolysis. A
13 model is outlined to define the ideal parameters and evaluate the annual performance of a
14 solar pyrolysis system. The model is demonstrated by considering a linear Fresnel reflector
15 (LFR) system operating in Seville, Spain. The ideal operating temperature and total residence
16 time were determined to be 571 K and 149 min, respectively. Subsequently, an LFR system
17 was sized to have a total reactor length of 3.23 m, a polar inclination angle of 39° and an
18 effective concentrating aperture area of 4.55 m². The maximum char yield fraction was found
19 to be 40.8 wt.%; however, the annual variability of the solar input resulted in the system
20 producing 1375 kg of biochar from 13.9 t of biomass. The model developed in this study can
21 be applied to evaluate a range of solar thermal technologies in other localities for producing
22 char, gas and oils through the pyrolysis process.

23
24 Keywords: linear Fresnel reflector (LFR); bioenergy; concentrating solar thermal power
25 (CSP); slow pyrolysis; kinetics.

38 Nomenclature

39

40	A	Pre-exponential factor (1/s)
41	A_c	Effective concentrating aperture area (m ²)
42	A_s	Area of biomass particle (m ²)
43	b	Time constant (-)
44	B_i	Biot number (-)
45	C_p	Specific heat capacity of biomass (J/kgK)
46	DNI	Direct normal irradiance (W/m ²)
47	D_p	Biomass particle diameter (m)
48	D_r	Reactor diameter (m)
49	$E_{a,cj}$	Activation energy of char reaction (kJ/mol)
50	$E_{a,tj}$	Activation energy of tar reaction (kJ/mol)
51	F_{rp}	View factor between the reactor wall and the biomass particles (-)
52	h_p	Enthalpy for pyrolysis (MJ/kg)
53	h_r	Height of reactor from concentrating elements (m)
54	h_{rad}	Radiation heat transfer coefficient between reactor wall and biomass (W/m ² K)
55	$IAM_{(\theta_t, \theta_l)}$	Incidence angle modifier (-)
56	k_b	Thermal conductivity of biomass feedstock (W/mK)
57	k_{cj}	Char-reaction rate coefficient for each biomass component (1/s)
58	k_{tj}	Tar-reaction rate coefficient for each biomass component (1/s)
59	L_{op}	Reactor length for processing feedstock at an ideal operating temperature (m)
60	$L_{reactor}$	Total reactor length (m)
61	L_{heat}	Reactor length for biomass heating (m)
62	\dot{m}_c	Mass flow of produced char (kg/s)
63	\dot{m}_g	Mass flow of produced gas (kg/s)
64	\dot{m}_j	Mass flow of each component (kg/s)
65	\dot{m}_{j0}	Mass flow of each component introduced into the reactor (kg/s)
66	\dot{m}_t	Mass flow of produced tar (kg/s)
67	Q_{in}	Heat delivered to solar receiver absorbing surface (W)
68	Q_{loss}	Heat loss (W)
69	Q_u	Heat gained by biomass particles (W)
70	R	Universal gas constant (kJ/molK)
71	T_a	Ambient temperature (K)
72	T_i	Initial biomass temperature (K)
73	T_{op}	Ideal operating temperature (K)
74	t_{op}	Residence time (s)
75	t_{perm}	Total residence time (s)
76	T_r	Reactor wall temperature (K)
77	t_{heat}	Time for biomass particles to reach ideal operating temperature (s)
78	U_L	Heat loss coefficient (W/m ² K)
79	\dot{V}	Feeding rate (m ³ /s)
80	V_s	Volume of each biomass particle (m ³)
81	X_{cj}	Char-gas mass proportions (-)
82	Y_c	Char yield fraction (%)
83	Y_j	Biomass component mass fraction (-)
84		
85	α_s	Solar altitude angle (degrees)
86	γ_s	Azimuth angle from the south (degrees)
87	ϵ_p	Biomass void fraction (-)

88	ε_r	Inner reactor wall emissivity (-)
89	$\eta_{0=\theta}$	Collector optical efficiency at normal incidence angle (%)
90	$\eta_{end-loss}$	End-loss efficiency (%)
91	η_{total}	Total optical efficiency (%)
92	θ	Incidence angle (degrees)
93	θ_l	Longitudinal angle (degrees)
94	θ_p	Collector inclination angle (degrees)
95	θ_t	Transversal angle (degrees)
96	ρ_s	Biomass density (kg/m ³)

97
98
99
100
101
102
103
104
105
106
107
108
109
110
111
112
113
114
115
116
117
118
119
120
121
122
123
124
125
126
127
128
129
130
131
132
133
134
135

136 **1. Introduction**

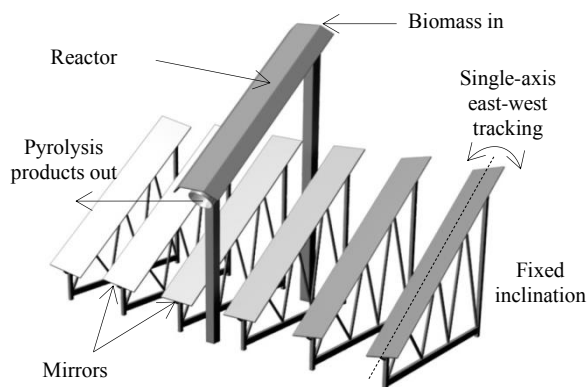
137 Pyrolysis involves the thermal degradation of a substance in the absence of oxygen. The
138 outputs from the process are gas and liquid products, and a carbon-rich solid residue called
139 char. Densifying biomass into a biochar through pyrolysis provides several benefits as it
140 increases energy density, reduces cost of transportation, makes it more grindable and
141 provides a more homogeneous product. Whilst biochar can be utilised as a solid fuel, it can
142 be used in a range of applications to achieve agricultural and environmental gains [1].
143 Biochar can be used for improving water retention and increasing soil fertility. Energy can be
144 generated from pyrolysis gas and liquid products and, as biochar acts as a long-term carbon
145 sink, there is the potential for systems to be carbon negative [2].

146
147 Slow pyrolysis, which involves relatively low temperatures (300-500 °C) and long residence
148 times (minutes to hours), produces comparable liquid, gas and biochar yields. Fast pyrolysis
149 (>500 °C) is used to increase the liquid fraction [3,4] and torrefaction (200-300 °C) is a mild
150 form of pyrolysis used primarily for char production [5]. Typically, electricity or fossil fuels
151 are used to provide the heat to a pyrolysis system, as the energy input can be easily
152 controlled. However, to improve the sustainability of pyrolysis systems, alternative
153 renewable energy sources are being investigated [6]. In hot rural areas there is an abundance
154 of solar energy and grid electricity is often unavailable or unreliable, thus there has been a
155 growing interest in the use of solar energy [7].

156
157 Concentrating solar thermal power (CSP) systems comprise a concentrator and a receiver.
158 Several authors have investigated using a solar concentrator to provide the heat input to a
159 receiver acting as a pyrolysis reactor. Morales et al. [8] evaluated the use of a parabolic
160 trough collector (PTC) for pyrolysis using ray-tracing, but they did not go on to consider the
161 impracticalities associated with solar tracking, off-axis rays and variable diurnal and seasonal
162 irradiance levels. A fast pyrolysis system using a parabolic dish reflector (PDR) was proposed
163 by Joardder et al. [9]. Their study focused on the biomass and solar resource availability in
164 Bangladesh. Zeng et al. [10] outlined a two-stage heliostat-PDR concentrator with a shutter
165 system for controlling heating rate and temperature of a pyrolysis reactor. Their study
166 addressed the effects of temperature (600-2000 °C) and heating rate (5-450 °C/s) on char
167 yield and properties, rather than on the performance of the system. Zeaiter et al. [11] built and
168 tested a solar pyrolysis system using a Fresnel lens with two-axis tracking. The system
169 reached temperatures of 550 °C and was used to pyrolyse waste rubber.

170 High temperature CSP systems have been examined for producing hydrogen and syngas.
171 Abanades et al. [12] looked at obtaining hydrogen through the pyrolysis of natural gas using
172 solar energy, and Kruesi et al. [13] studied solar gasification of bagasse. Z'Graggen &
173 Steinfeld [14] investigated the use of a solar furnace for hydrogen production via steam-
174 gasification, and they used a kinetic model to size the reactor and specify operational
175 parameters. Several other authors have considered using a CSP system to provide heat
176 indirectly for gasification processes [15-18]. Whilst an indirect system will increase cost and
177 complexity, it does offer improvements in control and stability.

178
179 Issues with using a CSP system to provide the heat input to a pyrolysis reactor arise due to
180 the variable nature of solar energy and the need for solar tracking. Additional difficulties are
181 caused when using a PTC and PDR system, as they use expensive fragile receivers that need
182 to move with the tracking system. An alternative CSP technology is the linear Fresnel
183 reflector (LFR), which is a relatively simple and inexpensive technology. The receiver tower
184 is fixed—removing the need for flexible hosing and a fragile evacuated tube—and insulates a
185 single pipe or multiple tubes. Biomass could, therefore, be fed into this heated pipe and
186 transformed into char, gas and pyrolysis oil products (see Figure 1). Unlike expensive
187 parabolically shaped mirrors, the LFR also uses low-cost flat mirror element segments that
188 can be rotated to control receiver temperature. However, an LFR's individual mirror elements
189 are normally driven by independent motors, which can increase complexity. Another
190 disadvantage of the LFR system is that it captures less energy than other solar collectors due
191 to a lower optical efficiency. As with all CSP systems, there is a need for research to provide
192 methods for sizing them for specific applications and evaluating daily and annual
193 performance.



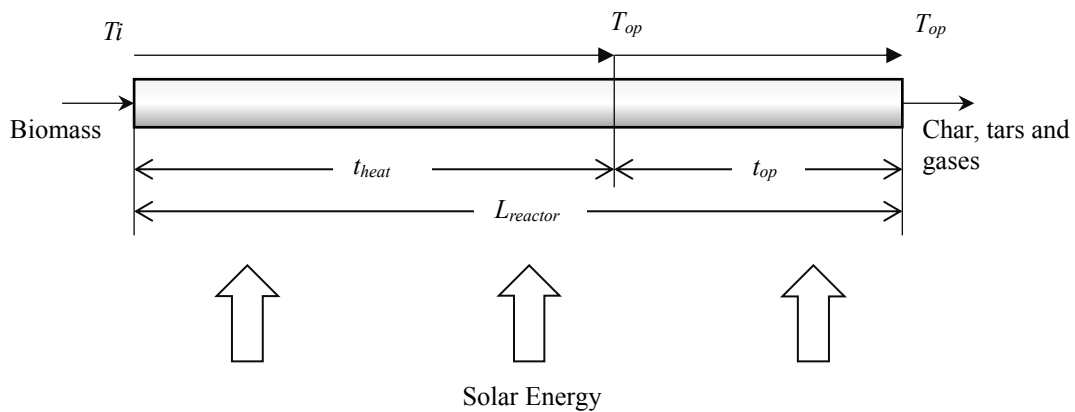
194
195 **Figure 1:** A linear Fresnel reflector with a polar alignment and east-west single-axis tracking.

196 This study aims to outline a theoretical model for sizing and evaluating the performance of
 197 solar pyrolysis systems by integrating pyrolysis kinetics, sun-earth geometry relations and
 198 solar thermal performance calculations. Using this model, the LFR technology and the impact
 199 of variable solar irradiance levels on biochar production and other system outputs is to be
 200 investigated. This will enable diurnal and seasonal changes in the product yields from a solar
 201 pyrolysis system to be modelled for specific locations.

202
 203 In the following section, the method used to achieve this study’s aim is outlined. In section 3,
 204 a model is developed for simulating solar pyrolysis reactions, and it is applied to a case study
 205 scenario in section 4. The paper concludes by evaluating the results and providing
 206 recommendations for future research on solar pyrolysis systems.

207
 208 **2. Method**

209 In a solar pyrolysis reactor, biomass particles will increase in temperature from an initial
 210 biomass temperature, T_i , and then undergo pyrolysis at an ideal operating temperature, T_{op} . In
 211 kinetic studies, the pyrolysis products formed before a feedstock reaches a desired operating
 212 temperature are often neglected [2]. Therefore, two processes can be considered: (i) heating
 213 of biomass particles inside a reactor from an ambient temperature to an operating
 214 temperature, and (ii) pyrolysis reactions occurring at the operating temperature (see Figure 2).



215
 216 **Figure 2:** A solar pyrolysis reactor heating biomass particles from an inlet temperature to an
 217 ideal operating temperature.

218
 219 The kinetic model adopted for this study is based on the works by Van der Weerdhof [19] and
 220 Miller and Bellan [20]. In this model, the individual cellulose, hemicellulose and lignin
 221 components, and their thermal decomposition into char, volatile tars and gases, are

222 considered. As cellulose, hemicellulose and lignin decompose at different rates and over
223 different temperature ranges [21], an ideal operating temperature, T_{op} , and residence time, t_{op} ,
224 for maximising char production can be determined. The total residence time is given by the
225 sum of a drying and heating residence time, t_{heat} (i.e. a period of time where biomass particles
226 are increasing in temperature) and a residence time, t_{op} , which is the length of time biomass is
227 processed at the operating temperature. In conventional reactors, the operating temperature
228 can be maintained; however, for a solar pyrolysis reactor, mean values have to be used to
229 calculate pyrolysis yields.

230

231 By simulating char production for varying operational temperatures and residence times, a
232 practical total length for the solar pyrolysis reactor, $L_{reactor}$, can be determined for a particular
233 feeding rate. The approach taken in this study is to simulate char production for increasing
234 temperatures and residence times until the yield increases by less than 10% in a one minute
235 period. At this point, the assumption is made that the ideal operating conditions have been
236 determined. The justification for this approach is that further increases in char production
237 rates would result in impracticalities associated with an excessive solar pyrolysis reactor
238 length.

239

240 The heat transferred to the biomass particles in the reactor is calculated by assuming a
241 lumped system approach outlined by Çengel [22]. A limitation of this approach is that it
242 assumes a uniform temperature inside the reactor. The heat transferred to the reactor from a
243 solar concentrator is determined using conventional CSP performance calculations [23].
244 Subsequently, the solar system can be sized to provide the required ideal operating
245 temperature at solar noon for a typical meteorological day. These specifications can be
246 achieved for different solar collectors and tracking arrangements.

247

248 To evaluate the annual performance of the sized solar pyrolysis system, it is assessed for a
249 typical meteorological year (TMY). Direct normal irradiance values are obtained from the
250 meteorological database, Meteonorm[®]. Thermal performance and incidence angle modifier
251 models for an LFR are presented based on previous studies by Nixon et al. [24-26].

252 MatLAB[®] is the software package used to run the simulations.

253

254 3. Model

255 The model outlined in this study is a generic model that could be adopted for any solar
256 collector and is divided into three parts: modelling (i) the pyrolysis process to determine char,
257 gas and tar yields, (ii) biomass particle heat transfer, and (iii) reactor heat gain and heat loss.

258

259 3.1 The pyrolysis process

260 Two different pyrolysis reactions are considered in the model: the char reaction, which
261 produces char and gases, and the tar reaction, which produces volatile tars. Assuming that the
262 pyrolysis of biomass follows first-order reaction kinetics, the mass flow of biochar produced,
263 \dot{m}_c , can be estimated by integrating the following equation [19]:

$$\frac{\partial \dot{m}_c}{\partial t} = \sum_j k_{cj} X_{cj} \dot{m}_j \quad (1)$$

264 The index j represents the cellulose, hemicellulose and lignin biomass components, and k_{cj} is
265 the char-reaction rate coefficient for each biomass component. X_{cj} represents the char-gas
266 mass proportions that are produced during the char-reaction and \dot{m}_j is the mass flow of each
267 component at a particular moment.

$$\dot{m}_j = \dot{m}_{j0} e^{-(k_{cj} + k_{tj})t_{op}} \quad (2)$$

268 The char-reaction rate coefficients and tar-reaction rate coefficients, k_{tj} , can be calculated
269 from the Arrhenius equation [27],

$$k_{cj} = A e^{-\frac{E_{a,cj}}{RT_{op}}} \quad (3)$$

$$k_{tj} = A e^{-\frac{E_{a,tj}}{RT_{op}}} \quad (4)$$

270 where A is a pre-exponential factor, E_a is the activation energy of the reaction, and R is the
271 universal gas constant.

272

273 As the pyrolysis process takes place, the mass of each biomass component decreases and the
274 mass of char formed increases. The mass flow of each component introduced into the reactor,
275 \dot{m}_{j0} , depends on the feedstock characteristics and the biomass feedstock feeding rate, \dot{V} ; it can
276 be expressed as,

277

$$\dot{m}_{j0} = (1 - \varepsilon_p)\rho_s Y_j \dot{V} \quad (5)$$

278 The feedstock dependent parameters are the biomass void fraction, ε_p , density, ρ_s , and
 279 cellulose, hemicellulose and lignin mass fractions, Y_j .

280

281 The char yield fraction, Y_c , can now be calculated as,

$$Y_c = \frac{\dot{m}_c}{\sum_j \dot{m}_{j0}} \quad (6)$$

282

283 By integrating Eq.1, the mass flow of char, \dot{m}_c , and gas, \dot{m}_g , produced can be obtained as a
 284 function of the residence time, t_{op} , and k_{cj} and k_{tj} , which depend on the reactor temperature,
 285 T_{op} .

286

$$\dot{m}_c = \sum_j \left[\frac{k_{cj} X_{cj} \dot{m}_{j0}}{k_{cj} + k_{tj}} - \frac{k_{cj} X_{cj} \dot{m}_{j0}}{k_{cj} + k_{tj}} \cdot e^{-(k_{cj} + k_{tj})t_{op}} \right] \quad (7)$$

287

$$\dot{m}_g = \sum_j \left[\frac{k_{cj}(1 - X_{cj})\dot{m}_{j0}}{k_{cj} + k_{tj}} - \frac{k_{cj}(1 - X_{cj})\dot{m}_{j0}}{k_{cj} + k_{tj}} \cdot e^{-(k_{cj} + k_{tj})t_{op}} \right] \quad (8)$$

288 Similarly, the mass flow of produced tar, \dot{m}_t , can be calculated.

$$\dot{m}_t = \sum_j \left[\frac{k_{tj} \dot{m}_{j0}}{k_{cj} + k_{tj}} - \frac{k_{tj} \dot{m}_{j0}}{k_{cj} + k_{tj}} \cdot e^{-(k_{cj} + k_{tj})t_{op}} \right] \quad (9)$$

289 By varying T_{op} , the mass flow of the pyrolysis products can be determined for different
 290 residence times. For each T_{op} value, a suitable residence time can be determined based on
 291 diminishing returns: i.e. a point where any additional pyrolysis product gains are not worth a
 292 further increase in residence time. A T_{op} value giving the highest mass flow of a particular
 293 pyrolysis component at the lowest t_{op} value can then be found in order to minimise reactor
 294 length. Having determined an ideal residence time and reactor temperature, the reactor length
 295 for processing biomass particles at the ideal operating temperature, L_{op} , can be specified for a
 296 particular reactor diameter, D_r .

$$L_{op} = \frac{4\dot{V}t_{op}}{\pi D_r^2} \quad (10)$$

297

298

299 3.2 Biomass particle heat transfer

300 A lumped system approach is used to describe the heating process that raises biomass
301 particles in the reactor from an initial temperature to an ideal operating temperature. The
302 approach is characterised by a Biot number, B_i , which depends on feedstock type and particle
303 diameter, and the method is considered to be valid for Biot numbers of less than 0.1 [22].

$$B_i = \frac{h_{rad}V_s}{k_bA_s} \quad (11)$$

304 V_s is the volume of each biomass particle, A_s is the area of each particle and k_b is the thermal
305 conductivity of the chosen biomass feedstock.

306

307 The radiation heat transfer coefficient between the reactor wall and the biomass particles,
308 h_{rad} , can be calculated from,

$$h_{rad} = \frac{\sigma(T_i^2 + T_r^2)(T_i + T_r)}{\frac{1}{\varepsilon_r} - 1 + \frac{1}{F_{rp}}} \quad (12)$$

309 where σ is the Stefan-Boltzmann constant, T_r is the reactor wall temperature, ε_r is the inner
310 reactor wall emissivity, and F_{rp} is the view factor between the reactor wall and the biomass
311 particles. The time required for particles to reach an ideal operating temperature, t_{heat} , can be
312 determined from,

$$t_{trans} = \frac{\ln\left(\frac{T_{op} - T_r}{T_i - T_r}\right)}{-b} \quad (13)$$

313

314 Parameter b is a time constant that is calculated from,

$$b = \frac{h_{rad}A_s}{\rho_s V_s C_p} \quad (14)$$

315 where C_p is the specific heat capacity of biomass.

316

317 The reactor length required for biomass heating, L_{heat} , can now be found:

$$L_{heat} = \frac{4\dot{V}t_{heat}}{\pi D_r^2} \quad (15)$$

318

319 The total reactor length, $L_{reactor}$, and total residence time, t_{perm} , are respectively calculated
 320 from $L_{heat} + L_{op}$ and $t_{heat} + t_{op}$.

321

322 **3.3 Heat gain and loss**

323 The heat gained by biomass particles, Q_u , in a reactor can be expressed by the following
 324 equation:

325

$$Q_u = h_{rad}\pi D_r L_{reactor}(T_r - T_i) \quad (16)$$

326

327 This assumes that the reactor is of uniform temperature, which, for solar systems, is only
 328 valid for low flow rates and short reactor lengths. If the temperature difference between the
 329 reactor wall and biomass particles is small, the heat gain found from Eq.(16) will be
 330 comparable to,

$$Q_u = \sum_j \dot{m}_{j0} C_p (T_{op} - T_i) \quad (17)$$

331 The required heat gain can be related to the enthalpy for pyrolysis, h_p , which defines the
 332 energy required to raise the feedstock from room temperature to reaction temperature, and
 333 convert the feedstock into pyrolysis products.

$$Q_u = \frac{h_p \rho_s (1 - \varepsilon_p) \frac{1}{4} \pi D_r^2 L_{reactor}}{t_{perm}} \quad (18)$$

334 The enthalpy for pyrolysis depends on reactor temperature due to changes in pyrolysis
 335 reaction chemistry, and enthalpy values stated in the literature have been calculated using
 336 different methods, feedstocks, reactor temperatures and assumptions regarding heat losses
 337 [28,29]. It is, therefore, difficult to use sensible and reaction enthalpies to determine an
 338 optimal operating temperature.

339 Assuming the reactor wall is of a uniform temperature, the heat loss, Q_{loss} , can be calculated
 340 from the ambient temperature, T_a , the solar-receiver geometry and a heat loss coefficient, U_L :

$$Q_{loss} = U_L \pi D_r L_{reactor} (T_r - T_a) \quad (19)$$

341 The heat loss coefficient is often expressed as a polynomial function of T_r .

$$U_L = a_2 T_r^2 - a_1 T_r + a_0 \quad (20)$$

342 Where an inert gas such as nitrogen is used for purging oxygen from the system, the heat
 343 transfer equations can be amended to include heating the gas and heat lost as the gas exits the
 344 system [28].

345 The energy delivered to a solar receiver's absorbing surface, Q_{in} , is given by,

$$Q_{in} = DNI \cdot A_c \cdot \eta_{(\theta=0)} \cdot IAM_{(\theta_t, \theta_l)} \cdot \eta_{end-loss} \quad (21)$$

346 where DNI is the direct normal irradiance, A_c is the effective concentrating aperture area of
 347 the collector, and $\eta_{\theta=0}$ is the optical efficiency of a collector when approaching rays are at a
 348 normal incidence angle, θ , to the aperture area. The optical efficiency includes properties
 349 such as transmittance, reflectance, absorbance and an intercept factor. These parameters
 350 depend on the sun's relative position to a solar system, so an Incidence Angle Modifier (IAM)
 351 is included to model daily and yearly changes in the optical efficiency. The IAM depends on
 352 the type of solar collector and tracking orientation being used, and it can be estimated from a
 353 product of the losses that occur due to off-axis rays in the transversal, θ_l , and longitudinal, θ_t ,
 354 planes [26,30]. For a north-south alignment,

355

$$\theta_t = 90 - \tan^{-1} \left(\frac{\tan \alpha_s}{\cos(90 - \gamma_s)} \right) \quad (22)$$

$$\theta_l = 90 - \theta_p - \tan^{-1} \left(\frac{\tan \alpha_s}{\cos \gamma_s} \right) \quad (23)$$

356 where γ_s is the azimuth angle from the south, α_s is the solar altitude angle, and θ_p is the
 357 collector's inclination angle from the horizontal (e.g. when a polar-axis is used).

358

359 As the collector will be of a short length, additional end-losses, $\eta_{end-loss}$ —which can be
 360 calculated from the height of the reactor from the concentrating elements, h_r —should be
 361 considered.

$$\eta_{end-loss} = 1 - \frac{h_r \tan \theta_l}{L_{reactor}} \quad (24)$$

362 The total optical efficiency, η_{total} , at any given time is found from,

$$\eta_{total} = \eta_{(\theta=0)} \cdot IAM_{(\theta_t, \theta_l)} \cdot \eta_{end-loss} \quad (25)$$

363 The required effective concentrating aperture area to heat the reactor to a specific ideal
 364 operating temperature can now be determined for solar noon on a typical day of the year. This
 365 is achieved by assuming that the energy delivered to the solar reactor, Q_{in} , equals the sum of
 366 the heat gained by the biomass particles, Q_u , and the heat lost by the reactor, Q_{Loss} . With the
 367 solar pyrolysis system sized, the performance can be investigated by simultaneously solving
 368 T_r to determine daily varying reactor temperatures during a typically meteorological year.

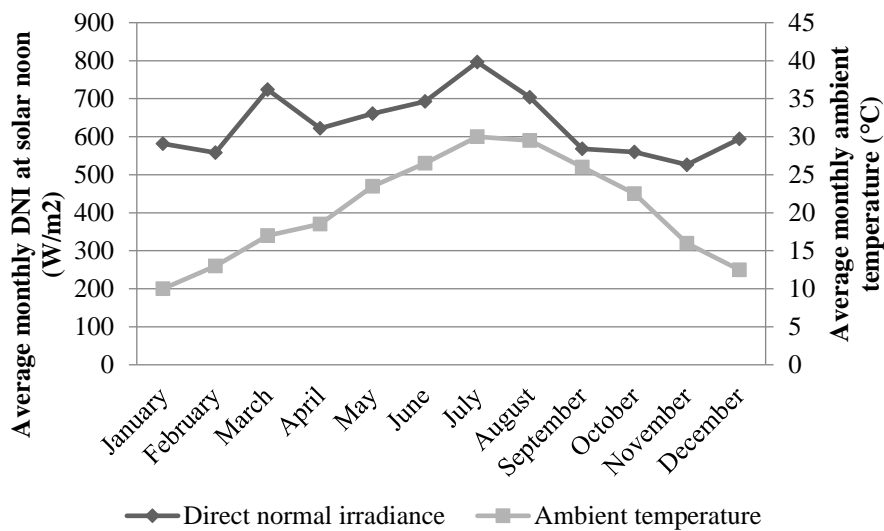
369

370 4. Application to case study

371 The model is used to evaluate the annual performance of a solar pyrolysis system based on
 372 the linear Fresnel reflector technology. The chosen location is Seville, Spain, and ten-minute
 373 direct normal irradiance values have been taken for a TMY using the meteorological database
 374 Meteonorm[®]. The latitude angle for Seville is 37° and Figure 3 shows typical monthly
 375 irradiance and ambient temperature values.

376

377



378

379 **Figure 3:** Average monthly direct normal irradiance values at solar noon and ambient
 380 temperatures in Seville, Spain.

381

382 For the LFR system, the collector's optical efficiency ($\eta_{\theta=\theta}$), reactor diameter and inner
 383 reactor wall emissivity are taken respectively as 75%, 70 mm and 0.18. In order to mitigate
 384 the effect of collector end-losses, the tracking orientation considered is a polar-axis with east-
 385 west tracking. The maximum reduction in annual end-losses is achieved by an inclination
 386 angle, θ_p , of 39°. For the purposes of this study, a uniform reactor wall temperature
 387 distribution is assumed and the difference between the reactor wall surface temperature and

388 the biomass particle temperature is taken as 10 °C. Differences in reactor wall and particle
 389 temperature have been evaluated in Ref. [31]. The reactor is assumed to process biomass in a
 390 vacuum and therefore the heat transfer properties associated with a purging agent are not
 391 considered.

392

393 The LFR's heat loss coefficient and $IAM_{(\theta_l, \theta_t)}$ are defined by,

394

$$U_L = 0.0000077.T_r^2 + 0.0042163.T_r + 0.5648278 \quad (26)$$

395

$$IAM_{\theta_t} = 0.9967692 - 0.0024524\theta_t + 0.0000925\theta_t^2 - 0.0000021\theta_t^3 \quad (27)$$

396

$$IAM_{\theta_l} = 1.0010489510 - 0.0050582751\theta_l + 0.0000682110\theta_l^2 - 0.0000060431\theta_l^3 + 0.0000000504\theta_l^4 \quad (28)$$

397

398 where $IAM_{(\theta_l, \theta_t)}$ is obtained from the product of IAM_{θ_t} and IAM_{θ_l} . The type of biomass to be
 399 processed is wood chip, comprising of 46% cellulose, 32% hemicellulose and 22% lignin
 400 mass fractions. The feeding rate for passing biomass through the solar pyrolysis reactor is set
 401 at 0.005 m³/h. The thermal conductivity, specific heat capacity and particle diameter of the
 402 biomass feedstock are assumed to be 2273 J/kg.K [32], 0.1 W/m.K [31] and 0.01 m,
 403 respectively. The model input parameters are summarised in Table 1 and the kinetic
 404 parameters used for the pyrolysis of wood chip are shown in Table 2.

405 **Table 1:** Model input parameters.

Parameter	Units	Value
Feeding rate (\dot{V})	m ³ /s	0.005
Cellulose mass fraction ($Y_{j, cel}$)	-	0.46
Hemicellulose mass fraction ($Y_{j, hem}$)	-	0.32
Lignin mass fraction ($Y_{j, lig}$)	-	0.22
Biomass density (ρ_s)	kg/m ³	1250
Biomass void fraction (ϵ_p)	-	0.55
Specific heat capacity of biomass (C_p)	J/(kgK)	2273
Biomass particle diameter (D_p)	m	0.01
Inner reactor wall emissivity (ϵ_r)	-	0.18
View factor (F_{rp})	-	1
Thermal conductivity of biomass (k_b)	W/(mK)	0.1
Radiation heat transfer coefficient (h_{rad})	W/(m ² K)	3.825
Biot Number (Bi)	-	0.06375

406

407

408

409 **Table 2:** Kinetic parameters for the pyrolysis of wood chip.

Kinetic parameter	Units	Cellulose	Hemicellulose	Lignin
<i>Char reaction</i>				
Activation energy of reaction (E_a)	(kJ/mol)	150.5	145.7	67.77
Pre-exponential factor (A)	(s^{-1})	1.3e10	2.6e11	1.15e3
Char-gas mass properties (X_{cj})	-	0.35	0.6	0.75
<i>Tar reaction</i>				
Activation energy of reaction (E_a)	(kJ/mol)	196.5	202.4	100.8
Pre-exponential factor (A)	(s^{-1})	3.28e14	8.75e15	2.19e3

410

411 **5. Results**

412 **5.1 Sizing the solar pyrolysis systems**

413 The initial results obtained from the model relate to the ideal system parameters to increase
 414 char production during a typical meteorological day. For the chosen case study location, the
 415 ideal operating temperature, T_{op} , and total residence time, t_{perm} , were determined to be 571 K
 416 and 8939 s (149 min), respectively. The heating rate was approximately 4 K min^{-1} . For a
 417 biomass feeding rate of 5 l/h, the solar system required a total reactor length, $L_{reactor}$, of 3.23
 418 m and an effective concentrating aperture area of 4.55 m^2 . Daugaard and Brown [28] suggest
 419 that enthalpies for biomass pyrolysis will be in the region of 0.8 to 1.8 MJ/kg. A value of 0.7
 420 MJ/kg has also been reported for wood chip being pyrolysed in a vacuum reactor [33]. Based
 421 on Eq.18, a temperature of 571 K would indicate an enthalpy of 1 MJ/kg, which correlates
 422 well with these findings.

423

424 The parameters of the sized system are summarised in Table 3.

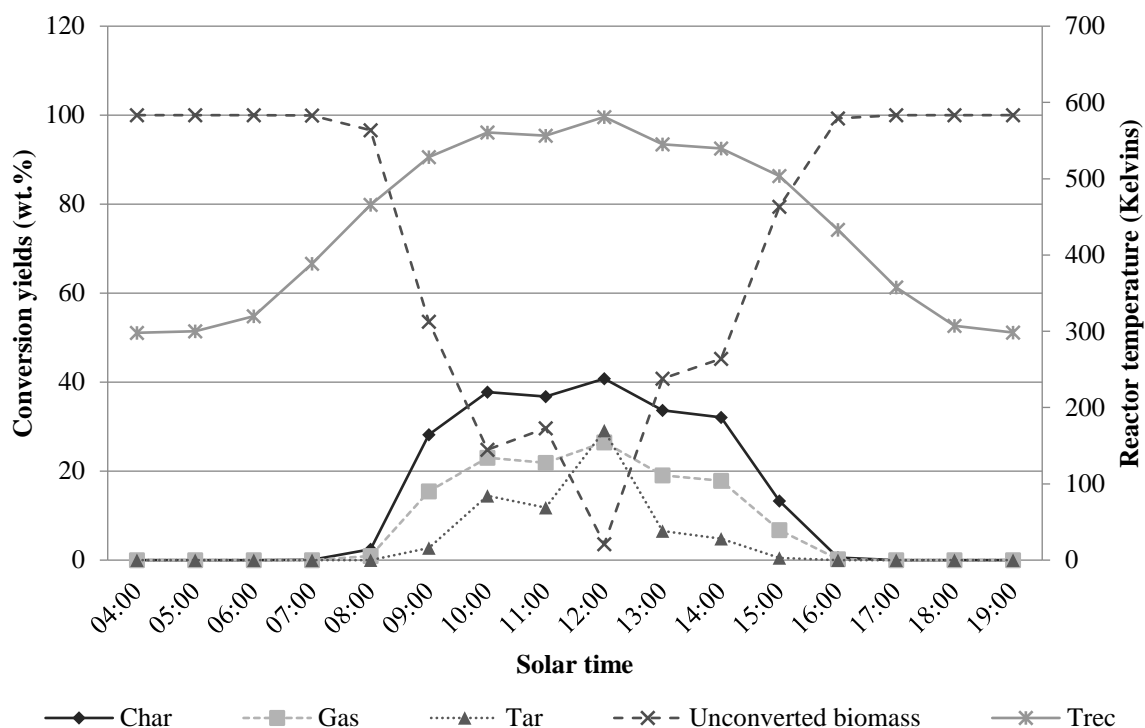
425

426 **Table 3:** Sized solar pyrolysis system parameters.

Parameter	Value	Units
Effective concentrating aperture area (A_c)	4.55	m^2
Reactor diameter (D_r)	0.07	m
Collector inclination angle (θ_p)	39	$^\circ$
Ideal temperature for pyrolysis (T_{op})	571	K
Reactor temperature (T_r)	581	K
Residence time (t_{op})	4800	s
Heating residence time (t_{heat})	4139	s
Total residence time (t_{perm})	8939	s
Permanent length of reactor (L_{op})	1.732	m
Heating length of reactor (L_{heat})	1.494	m
Total reactor length ($L_{reactor}$)	3.226	m
Height of reactor (h_r)	2.5	m

427

428 Figure 4 shows the performance of the system in terms of the conversion yields during a
 429 typical meteorological day in Seville, Spain. Potential pyrolysis product yields are compared
 430 for different operating temperatures achieved at specific times during the day. For the
 431 conditions achieved at solar noon, the maximum potential char yield obtained was found to
 432 be 40.8 wt.%; the gas and tar yields were 26.5 wt.% and 29.1 wt.%, respectively. These
 433 maximum yields cannot be obtained as the optimal conditions only occur at midday and the
 434 total residence time is 2.48 hrs. For the case study system, 49.5 kg of biomass can be fed into
 435 the system on a typical day, but only 6.4 kg of char would be obtained as the average daily
 436 char conversion yield would be 13 wt.%.
 437



438 Char Gas Tar Unconverted biomass Trec

439 **Figure 4:** Char, gas and tar percentage yields of fed biomass for a typical day in Seville,
 440 Spain. The temperature of the solar reactor is shown on the secondary axis.

441

442 5.2 Evaluation of annual performance

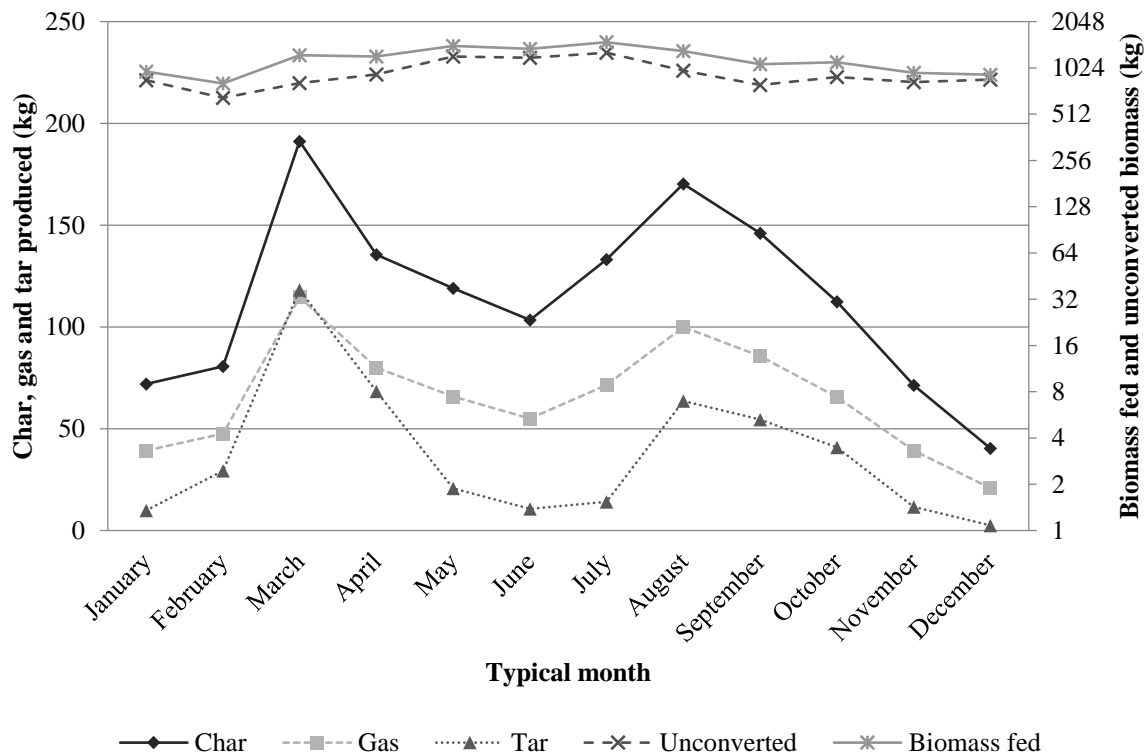
443 The monthly quantities of char, gas and tar produced from the system are shown in Figure 5.
 444 Total char produced was found to be 1375 kg from 13.9 t of fed biomass, which is an average
 445 annual conversion of 10.1 wt.%. As the ideal char conversion efficiency was determined to be
 446 40.8 wt.%, the annual variability of the solar input resulted in a 30 wt.% reduction in
 447 conversion efficiency. During July, the operational hours were at a maximum and the amount
 448 of biomass fed into the system was 1504 kg, which resulted in 133 kg of char being

449 produced. In March, 1241 kg was fed into the system and in August the input was 1315 kg.
 450 Even though a smaller amount of biomass was fed into the system during March and August,
 451 char yields were significantly higher at 191 kg and 170 kg, respectively.

452

453 The peak yields shown in Figure 5 for March and August are a result of the tracking
 454 orientation considered in this study. For a collector with a polar alignment and single-axis
 455 east-west tracking (see Figure 1), the incidence angle losses and end losses are lower when
 456 the sun is near the equinoxes. Therefore, even though the DNI is highest in July (see Figure
 457 3) and more biomass can be fed into the system due to more operational daylight hours, the
 458 total yield of pyrolysis products is reduced. In the winter months, a low DNI and high
 459 incidence angle losses result in very small yields.

460



461

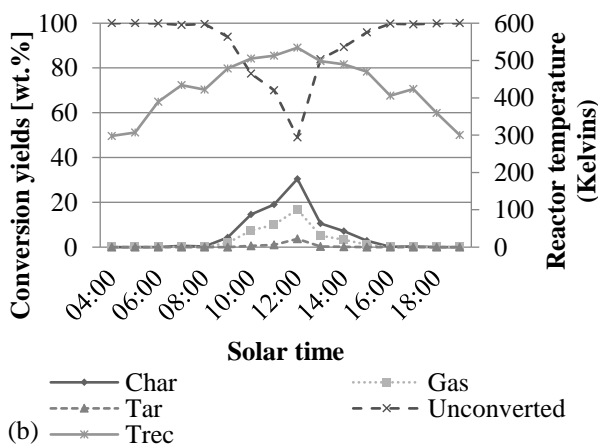
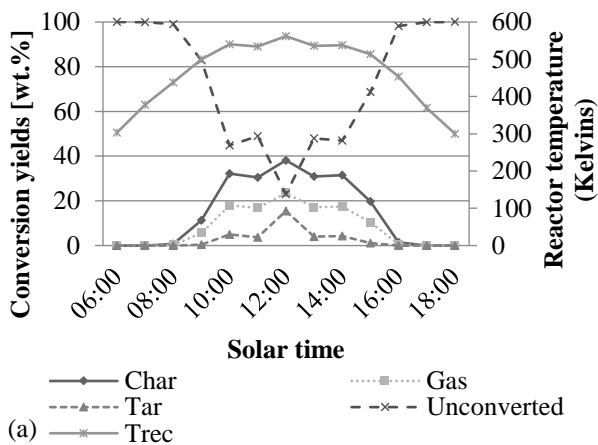
462 **Figure 5:** Char, gas and tar produced during a typical meteorological year in Seville, Spain.

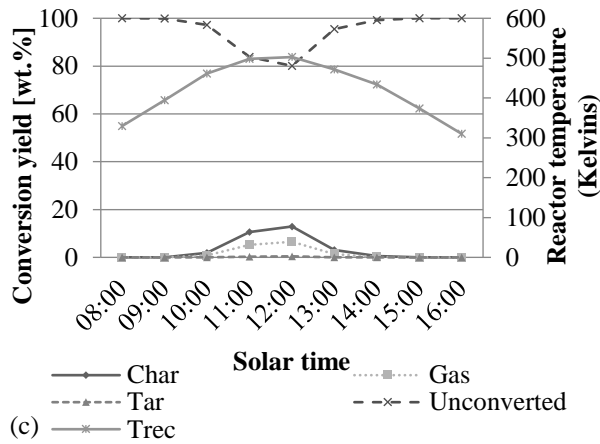
463 The secondary axis shows the amount of unconverted biomass and the amount of biomass fed
 464 into the system during these months.

465

466 To further examine the system's annual performance, Figure 6a-c shows the hourly char, gas
 467 and tar yields against reactor temperature for typical days in March, June and December. The
 468 system performance in March is comparable to a typical annual meteorological day (Figure
 469 4) as the sun is near the equinox during this month and perpendicular to the effective

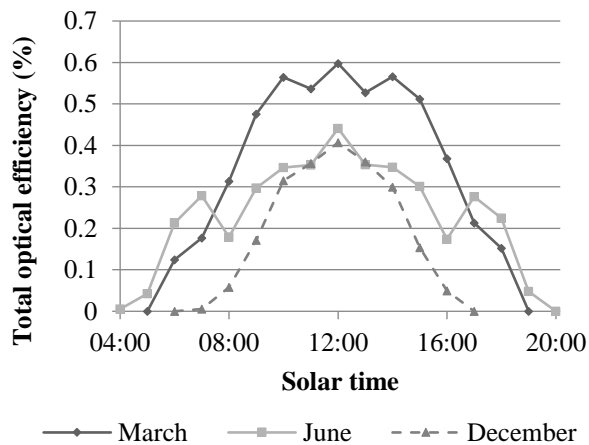
470 collector aperture area at solar noon. This results in a high total optical efficiency. Figure 6b
 471 shows that in June the char conversion at solar noon drops to 30 wt.% and yields drop rapidly
 472 either side of solar noon, as incident angle losses cause the reactor temperature to fall below
 473 500 K. In December, DNI values at solar noon are still reasonably high at 600 W/m²;
 474 however, the reactor temperature peaks at 500 K and quickly drops due to fewer daylight
 475 hours and high incidence angle losses. Consequently, char conversion yields reach only 12.9
 476 wt.% at solar noon and the majority of the feedstock remains unconverted. The combined
 477 influence of end losses and longitudinal and transversal incident angle losses on the daily
 478 total optical efficiencies in March, June and December can be seen in Figure 7. In June, the
 479 total optical efficiency is 44% at solar noon, whereas the total optical efficiency in March
 480 remains significantly higher at 60%.
 481





484
485
486
487
488

Figure 6a-c: Daily char, gas and tar yields for a solar pyrolysis reactor operating in Seville, Spain during a typical meteorological day in (a) March, (b) June and (c) December.



489
490
491
492

Figure 7: Total optical efficiency for the case study LFR system operating in Seville, Spain during a typical meteorological day in March, June and December.

493 6. Discussion

494 The peak char yield of 40.8 wt.% has a good agreement with yield values reported elsewhere
495 for slow pyrolysis [2]. A total residence time of 149 min is a moderately high value for solar
496 pyrolysis, and a reactor temperature of 581 K and a heating rate of 4 K min⁻¹ are relatively
497 low; however, these parameters are within the ranges reported in the literature [6]. The long
498 residence time can be attributed to the low radiation heat transfer coefficient, which could be
499 improved with a higher inner reactor wall emissivity. The high char, gas and tar yield
500 fractions in the months of March and August are expected: incidence angle losses will be at a
501 minimum near the equinoxes for solar collectors with a polar-axis tracking orientation.
502 Therefore, even though DNI values are higher in summer months, the energy captured by the

503 solar system is reduced. The low values for winter months are due to reduced direct normal
504 irradiance values and fewer daylight operating hours. Whilst the average annual char yield
505 was only 10.1 wt.%, it is worth noting that annual conversion rates would be significantly
506 improved if biomass was not fed into the system until a minimum specified reactor
507 temperature were achieved; however, the total char produced would be reduced.

508

509 The financial implications of operating the system during periods of low irradiance would
510 need to be assessed. The case study presented in this paper was based on the use of wood
511 chips, which would need to be purchased, and low cost waste feedstocks would have different
512 yield outputs. The sized solar system is relatively small at a length of 3.22 m and with an
513 effective concentrating aperture area of 4.55 m². Thus, the system could be relatively cheap to
514 construct. In hot rural developing areas—where electricity maybe unavailable and there is an
515 abundance of agro-residues—1375 kg of biochar would be a valuable product for agricultural
516 gains, and the other system outputs would be more usable for energy applications than raw
517 waste feedstock.

518

519 The results presented in this study are highly dependent on the model assumptions, the
520 tracking orientation considered and the type of solar collector. The model assumes a uniform
521 temperature distribution and that pyrolysis reactions do not occur before biomass particles
522 reach a specified ideal operating temperature. Whilst these are common assumptions in
523 kinetic models for pyrolysis, it would be interesting to compare theoretical results with
524 experimental findings. Furthermore, in a solar pyrolysis reactor, hot spots on the receiver
525 would occur and biomass particles could exceed desired processing temperatures. A two-axis
526 tracking arrangement would greatly improve pyrolysis products yields and reduce optical
527 efficiency losses; however, it would involve a moving reactor and significantly increase
528 complexity.

529

530 As with all pyrolysis reactors, additional equipment would be needed to separate out the
531 different products. Pyrolysis oils and non-condensable gases can be separated in a condenser
532 with further clean-up operations performed depending on the intended downstream
533 application. Separating the char and unconverted biomass could be difficult and it would
534 involve the use of gravity separators. Although this could add expense and complexity to the
535 system, the model could be amended to consider unconverted feedstock being recycled and
536 fed back into the system. This would improve system performance during periods of low

537 solar energy input. Alternatively, the entire solid yield could be fed back into the system when
538 char yields are significantly low or a fraction of the mixture could be combusted to provide
539 an additional heat input. Another extension to the model would be to consider higher feeding
540 rates and controlling the feed rate to maintain a more constant reactor temperature. In further
541 work, the techno-economic feasibility of different system configurations could also be
542 investigated. Rather than designing a solar pyrolysis system for a typical meteorological day,
543 different parameters could be used. For example, the system could be oversized using a
544 concept such as the solar multiple and different tracking orientations could be compared. The
545 benefit of the model outlined in this study is that it can be easily adopted by other researchers
546 to investigate and compare different CSP technologies, system configurations and localities.

547

548

549 **7. Conclusion**

550 A model for sizing and evaluating solar pyrolysis systems has been outlined and applied to a
551 configuration comprising a linear Fresnel reflector with a polar axis east-west tracking
552 orientation. At solar noon, on a typical metrological day in Seville, Spain, a maximum char
553 yield of 40.8 wt.% was obtained. The influence of variable irradiance levels resulted in an
554 annual average char yield of 10.1 wt.%. We consider the LFR system to be a promising
555 option for producing biochar, as it has many benefits as a solar pyrolysis reactor in
556 comparison to more conventional concentrating solar thermal systems.

557

558 **Figures and tables**

559 **Figure 1:** A linear Fresnel reflector with a polar-axis tracking orientation.

560 **Figure 2:** A solar pyrolysis reactor heating biomass from an inlet temperature to an ideal
561 operating temperature.

562 **Figure 3:** Average monthly direct normal irradiance values at solar noon and ambient
563 temperatures in Seville, Spain.

564 **Figure 4:** Char, gas and tars percentage yields of fed biomass for a typical day in Seville,
565 Spain. The temperature of the solar reactor is shown on a secondary axis.

566 **Figure 5:** Char, gas and tars produced for a typical meteorological year. The secondary axis
567 shows the amount of unconverted biomass and the amount of biomass fed into the system
568 during these months.

569 **Figure 6a-c:** Daily char, gas and tar yields for a solar pyrolysis reactor operating in Seville,
570 Spain during a typical meteorological day in (a) March, (b) June and (c) December.

571 **Figure 7:** Total optical efficiency for the case study LFR system operating in Seville, Spain
572 during a typical meteorological day in March, June and December.

573 **Table 1:** Model input parameters.

574 **Table 2:** Kinetic parameters of wood chip.

575 **Table 3:** Sized solar pyrolysis system parameters.

576

577 **References**

578 [1] Manyà JJ. Pyrolysis for biochar purposes: a review to establish current knowledge gaps
579 and research needs. *Environ Sci Technol* 2012;46:7939-54.

580 [2] Hornung A. *Transformation of Biomass: Theory to Practice.* : John Wiley & Sons, 2014.

581 [3] Bruun EW, Ambus P, Egsgaard H, Hauggaard-Nielsen H. Effects of slow and fast
582 pyrolysis biochar on soil C and N turnover dynamics. *Soil Biol Biochem* 2012;46:73-9.

583 [4] Duman G, Okutucu C, Ucar S, Stahl R, Yanik J. The slow and fast pyrolysis of cherry
584 seed. *Bioresour Technol* 2011;102:1869-78.

585 [5] Batidzirai B, Mignot APR, Schakel WB, Junginger HM, Faaij APC. Biomass torrefaction
586 technology: Techno-economic status and future prospects. *Energy* 2013;62:196-214.

587 [6] Goyal HB, Seal D, Saxena RC. Bio-fuels from thermochemical conversion of renewable
588 resources: A review. *Renewable and Sustainable Energy Reviews* 2008;12:504-17.

589 [7] Panwar NL, Kaushik SC, Kothari S. Role of renewable energy sources in environmental
590 protection: A review. *Renewable and Sustainable Energy Reviews* 2011;15:1513-24.

591 [8] Morales S, Miranda R, Bustos D, Cazares T, Tran H. Solar biomass pyrolysis for the
592 production of bio-fuels and chemical commodities. *J Anal Appl Pyrolysis* 2014;109:65-78.

593 [9] Joardder MH, Halder PK, Rahim A, Paul N. Solar Assisted Fast Pyrolysis: A Novel
594 Approach of Renewable Energy Production. *Journal of Engineering* 2014.

595 [10] Zeng K, Minh DP, Gauthier D, Weiss-Hortala E, Nzihou A, Flamant G. The effect of
596 temperature and heating rate on char properties obtained from solar pyrolysis of beech wood.
597 *Bioresour Technol* 2015;182:114-9.

598 [11] Zeaiter J, Ahmad MN, Rooney D, Samneh B, Shammam E. Design of an automated solar
599 concentrator for the pyrolysis of scrap rubber. *Energy Conversion and Management*
600 2015;101:118-25.

601 [12] Abanades S, Tescari S, Rodat S, Flamant G. Natural gas pyrolysis in double-walled
602 reactor tubes using thermal plasma or concentrated solar radiation as external heating source.
603 *Journal of natural gas chemistry* 2009;18:1-8.

604 [13] Kruesi M, Jovanovic ZR, Steinfeld A. A two-zone solar-driven gasifier concept: Reactor
605 design and experimental evaluation with bagasse particles. *Fuel* 2014;117:680-7.

- 606 [14] Z'Graggen A, Steinfeld A. Hydrogen production by steam-gasification of carbonaceous
607 materials using concentrated solar energy—V. Reactor modeling, optimization, and scale-up.
608 Int J Hydrogen Energy 2008;33:5484-92.
- 609 [15] Ravaghi-Ardebili Z, Manenti F, Corbetta M, Pirola C, Ranzi E. Biomass gasification
610 using low-temperature solar-driven steam supply. Renewable Energy 2015;74:671-80.
- 611 [16] Hathaway BJ, Honda M, Kittelson DB, Davidson JH. Steam gasification of plant
612 biomass using molten carbonate salts. Energy 2013;49:211-7.
- 613 [17] Nickerson TA, Hathaway BJ, Smith TM, Davidson JH. Economic assessment of solar
614 and conventional biomass gasification technologies: Financial and policy implications under
615 feedstock and product gas price uncertainty. Biomass Bioenergy 2015;74:47-57.
- 616 [18] Tanaka Y, Mesfun S, Umeki K, Toffolo A, Tamaura Y, Yoshikawa K. Thermodynamic
617 performance of a hybrid power generation system using biomass gasification and
618 concentrated solar thermal processes. Appl Energy 2015;160:664-72.
- 619 [19] Van der Weerdhof MW. Modelling the pyrolysis process of biomass particles. 2010.
- 620 [20] Miller R, Bellan J. A generalized biomass pyrolysis model based on superimposed
621 cellulose, hemicellulose and lignin kinetics. Combustion Sci Technol 1997;126:97-137.
- 622 [21] Jahirul MI, Rasul MG, Chowdhury AA, Ashwath N. Biofuels production through
623 biomass pyrolysis—a technological review. Energies 2012;5:4952-5001.
- 624 [22] Cengel YA, Hernán Pérez J. Heat transfer: a practical approach. Transferencia de calor/
625 2004.
- 626 [23] Duffie JA, Beckman WA. Solar engineering of thermal processes. 3rd ed. New York:
627 John Wiley & Sons, 2006.
- 628 [24] Nixon JD, Dey PK, Davies PA. Design of a novel solar thermal collector using a multi-
629 criteria decision-making methodology. J Clean Prod 2013;59:150-9.
- 630 [25] Nixon J, Davies P. Construction and Experimental Study of an Elevation Linear Fresnel
631 Reflector. Journal of Solar Energy Engineering 2016;138:031001.
- 632 [26] Nixon JD, Davies PA. Cost-exergy optimisation of linear Fresnel reflectors. Solar
633 Energy 2012;86:147-56.
- 634 [27] Luo Z, Wang S, Cen K. A model of wood flash pyrolysis in fluidized bed reactor.
635 Renewable Energy 2005;30:377-92.
- 636 [28] Daugaard DE, Brown RC. Enthalpy for pyrolysis for several types of biomass. Energy
637 Fuels 2003;17:934-9.
- 638 [29] Atsonios K, Panopoulos KD, Bridgwater AV, Kakaras E. Biomass fast pyrolysis energy
639 balance of a 1kg/h test rig. International Journal of Thermodynamics 2015;18:267-75.
- 640 [30] Morin G, Dersch J, Platzer W, Eck M, Häberle A. Comparison of Linear Fresnel and
641 Parabolic Trough Collector power plants. Solar Energy 2012;86:1-12.
- 642 [31] Ellens CJ. Design, optimization and evaluation of a free-fall biomass fast pyrolysis
643 reactor and its products. 2009.

- 644 [32] Shackley S, Hammond J, Gaunt J, Ibarrola R. The feasibility and costs of biochar
645 deployment in the UK. *Carbon Management* 2011;2:335-56.
- 646 [33] Roy C, Lemieux R, de Caumia B, Blanchette D. Processing of wood chips in a
647 semicontinuous multiple-hearth vacuum-pyrolysis reactor. In: Anonymous : ACS
648 Publications; 1988.
- 649